

Self-Assembly and Secondary Structures of Linear Polypeptides Tethered to Polyhedral Oligomeric Silsesquioxane Nanoparticles Through Click Chemistry

YUNG-CHIH LIN, SHIAO-WEI KUO

Department of Materials and Optoelectronic Science, Center for Nanoscience and Nanotechnology, National Sun Yat-Sen University, Kaohsiung, Taiwan

Received 7 January 2011; accepted 21 February 2011

DOI: 10.1002/pola.24640

Published online 17 March 2011 in Wiley Online Library (wileyonlinelibrary.com).

ABSTRACT: In this study, we used click chemistry to synthesize a new macromolecular self-assembling building blocks, linear polypeptide-*b*-polyhedral oligomeric silsesquioxane (POSS) copolymers, from a mono-azido-functionalized POSS (N₃-POSS) and several alkyne-poly(γ -benzyl-L-glutamate) (alkyne-PBLG) systems. The incorporation of the POSS unit at the chain end of the PBLG moiety allowed intramolecular hydrogen bonding to occur between the POSS and PBLG units, thereby enhancing the α -helical conformation in the solid state, as determined through Fourier transform infrared spectroscopy and wide-angle X-ray diffraction analyses. POSS-*b*-PBLG underwent hierarchical

self-assembly, characterized using small-angle X-ray scattering, to form a bilayer-like nanostructure featuring α -helical or β -sheet conformations and POSS aggregates. Thermogravimetric analysis indicated that the thermal degradation temperature increased significantly after incorporation of the POSS moiety, which presumably formed an inorganic protection layer on the nanocomposite's surface. © 2011 Wiley Periodicals, Inc. *J Polym Sci Part A: Polym Chem* 49: 2127–2137, 2011

KEYWORDS: block copolymers; nanocomposites; polypeptides; POSS; self-assembly

INTRODUCTION Polypeptides have received much attention recently because of their potential applications in various scientific fields, their close relationship to proteins, their flexibility in terms of functionality, and their molecular recognition properties.^{1–4} The secondary structures of peptide chains play crucial roles in the formation of the well-defined tertiary structure of proteins.⁵ Because of its α -helical secondary structure, poly(γ -benzyl-L-glutamate) (PBLG) has a significant effect on the formation of hierarchically ordered structures. α -Helical PBLG units serve as rigid rod-like structures in the solid state and in solution,⁶ resulting in unique behavior such as thermotropic liquid crystalline ordering^{7,8} and thermoreversible gelation,^{9,10} respectively.

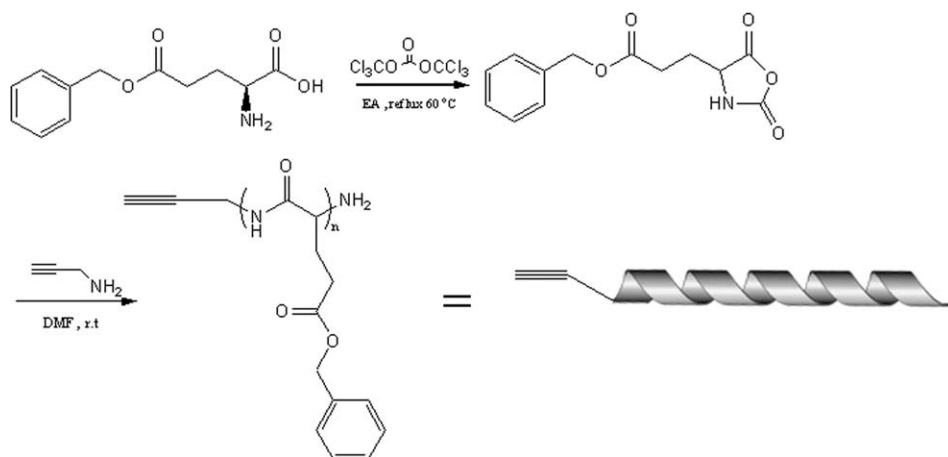
Performing conformational studies of model polypeptides is an important step on the road toward mimicking the biological activity of more complex proteins.¹¹ Indeed, there are many reported methods available for synthesizing polypeptide-*b*-nonpeptide (rod-coil) block copolymers based on rigid PBLG helices.^{12–22} The polypeptide domains in these systems are typically obtained from an amino-terminated polymer through ring-opening polymerization (ROP) of α -amino acid *N*-carboxyanhydride (NCA) monomers. In a previous study,²³ we combined the well-defined macromolecular architectures of polyhedral oligomeric silsesquioxane (POSS) and PBLG to generate polymeric building blocks having distinct three-

dimensional (3D) architectures for the self-assembly of supramolecular structures through the ROP of γ -benzyl-L-glutamate *N*-carboxyanhydride (γ -Bn-Glu NCA) using aminopropyl isobutyl-POSS as a macroinitiator. Because of POSS's unique structure, it is a useful building block for the preparation of a variety of nanostructured materials.^{24–32} The presence of a POSS moiety at the chain end allowed intramolecular hydrogen bonding to occur between the POSS and PBLG units, thereby enhancing the latter's α -helical conformation in the solid state, as characterized using infrared, Raman, and solid state NMR spectroscopy.²³ Nevertheless, because we had prepared this POSS-*b*-PBLG system through the so-called divergence or "graft from" method, it was difficult to distinguish how the POSS nanoparticles influenced the secondary structure of PBLG.³³

As a result, in this study we used the convergence or coupling method to synthesize linear PBLG-*b*-POSS copolymers through click chemistry. First, we synthesized alkyne-PBLG species with different degrees of polymerization through ROP of γ -Bn-Glu NCA using propargylamine as a macroinitiator (Scheme 1). Next, we synthesized linear PBLG-*b*-POSS copolymers from a mono-azido-functionalized POSS (N₃-POSS) and the alkyne-PBLG species using a click reaction (Scheme 2). Finally, we used differential scanning calorimetry (DSC), thermogravimetric analysis (TGA), Fourier

Correspondence to: S.-W. Kuo (E-mail: kuosw@faculty.nsysu.edu.tw)

Journal of Polymer Science Part A: Polymer Chemistry, Vol. 49, 2127–2137 (2011) © 2011 Wiley Periodicals, Inc.



SCHEME 1 Synthesis of alkyne-PBLG species.

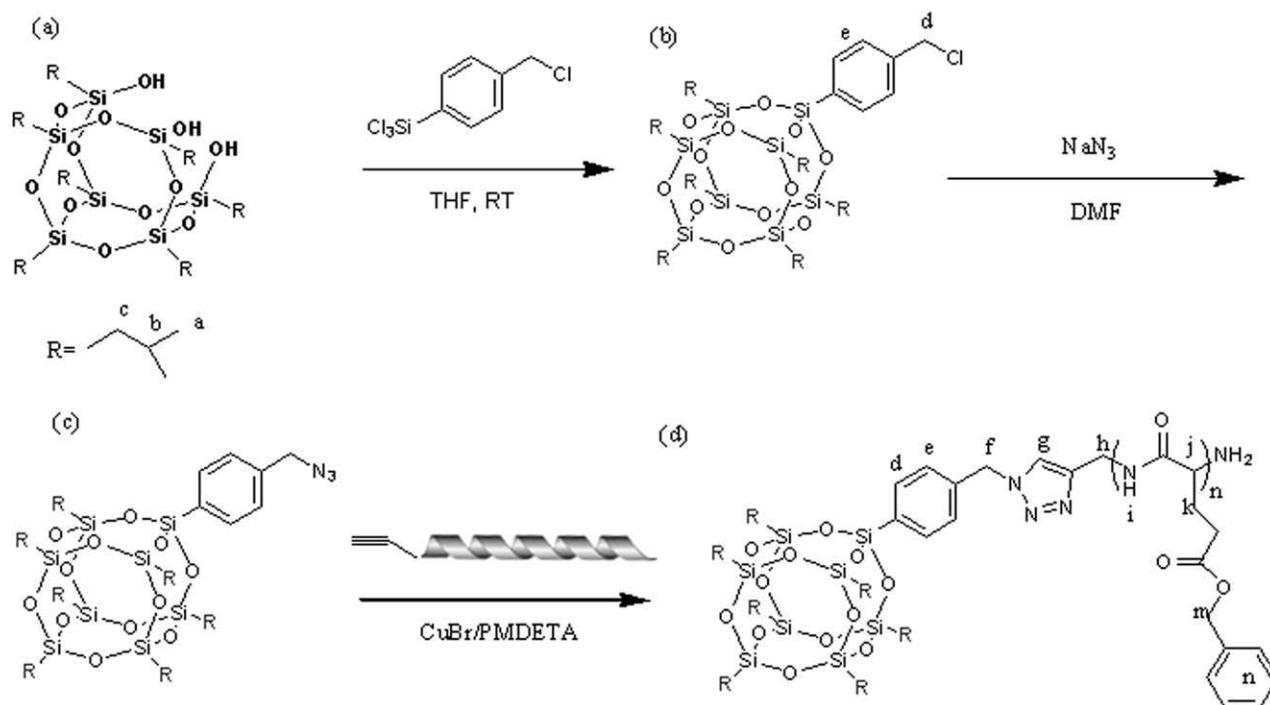
transform infrared (FTIR) spectroscopy, wide-angle X-ray diffraction (WAXD), and small-angle X-ray scattering (SAXS) to characterize the thermal properties, self-assembly, and secondary structures of the PBLG units.

RESULTS AND DISCUSSION

Synthesis of N_3 -POSS

N_3 -POSS was prepared through the corner-capping reaction of trichloro[4-(chloromethyl)phenyl]silane and isobutyltrisilanol-POSS and subsequent substitution with NaN_3 . Figure 1(a) presents FTIR spectra of the isobutyltrisilanol-POSS, mono-benzyl chloride POSS, and N_3 -POSS, recorded at room temperature. The spectrum of mono-benzyl chloride POSS [Fig. 1(a,b)] reveals that the signal for the OH group of isobutyltrisilanol-POSS had totally disappeared, indicating that

the corner-capping reaction had reached completion. The substitution of the chloride atom with the azido group led to the appearance [Fig. 1(a-c)] of a stretching vibration band for the azido group at 2102 cm^{-1} , confirming that N_3 -POSS had been obtained. The complete substitution of chloride atoms by azido groups was also confirmed in the ^1H NMR spectrum in Figure 1(b). After the substitution reaction, the signal of the benzyl CH_2 group connected to the chloride atom (4.60 ppm) shifted to higher field (4.36 ppm) for the benzyl azide. The lack of any remnant signal at 4.60 ppm suggested that the substitution reaction had reached completion. Figure 2 presents the ^{29}Si NMR spectrum of the mono-benzyl chloride POSS; we assign the resonances at -55.44 , -67.61 , -68.27 , and -81.27 ppm to the silicon nuclei of the silsesquioxane.³⁴ The ratio of the integration intensities of the signals for these silicon atoms confirmed that the



SCHEME 2 Synthesis of POSS-*b*-PBLG species.

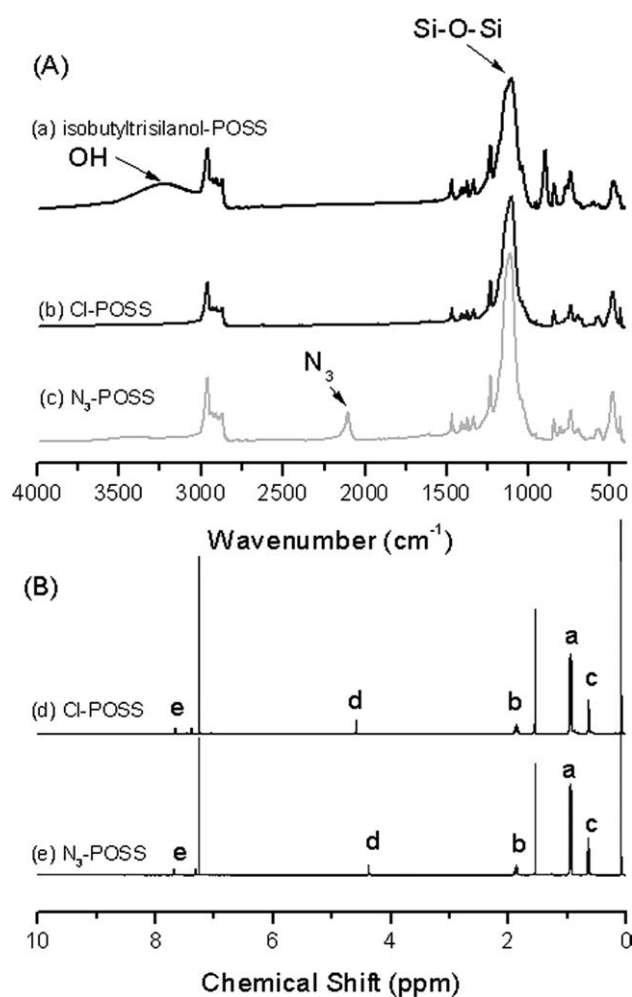


FIGURE 1 (A) FTIR spectra of (a) isobutyltrisilanol-POSS, (b) Cl-POSS, and (c) N_3 -POSS. (B) 1H NMR spectra of (d) Cl-POSS and (e) N_3 -POSS in $CDCl_3$.

octahedral silsesquioxane was obtained. In addition, the chemical shifts of the signals in the ^{29}Si NMR spectrum of N_3 -POSS were identical to those of its precursor, implying that the cage structure of N_3 -POSS was the same as that of the mono-benzyl chloride POSS. Thus, the complete cubic structure of the siloxane cage remained unchanged during the synthesis.

Synthesis of Alkyne-PBLG

Figure 3(a) presents the 1H NMR spectrum of the BLG monomer in $CDCl_3$. The benzyloxycarbonyl ring protons appeared as signals between 7.31 and 7.38 ppm, whereas the benzylic protons appeared as a doublet at 5.11 ppm. We assign the singlet at 6.4 ppm to the proton on the ring nitrogen atom; the other alkyl CH_2 protons appeared upfield as multiplets between 2.0 and 2.6 ppm. Figure 3(b) displays the 1H NMR spectrum of alkyne-PBLG in a mixture of $CDCl_3$ and 15% TFA. The signal for the proton on the nitrogen atom of alkyne-PBLG appeared as a singlet at 7.9 ppm; the singlets at 2.6 and 4.0 ppm correspond to the $C\equiv C-H$ and $C\equiv CCH_2$ protons, respectively; the aromatic protons appear as multi-

plets at 7.31–7.38 ppm. We determined the molar masses of alkyne-PBLG using the 1H NMR spectra and the following equation:

$$M_{n,PBLG} = \frac{I_b M_{BLG}}{I_f} + M_{propargylamine}$$

where I_b and I_f represent the intensities of the CH_2 protons b (alkyne-PBLG) from the PBLG main chain and the CH_2 protons f of the propargylamine initiator, respectively, and $M_{propargylamine}$ is the molar mass of the propargylamine initiator.³³ Table 1 lists the molecular weights of the various alkyne-PBLG systems, as determined through 1H NMR spectroscopic and GPC analyses.

Synthesis of Linear POSS-*b*-PBLG Copolymers

Figure 4 presents 1H NMR spectra of N_3 -POSS, alkyne-PBLG, and linear POSS-*b*-PBLG. Figures 1(b) and 3 provide the peak assignments for the spectra of alkyne-PBLG and N_3 -POSS; Scheme 2(d) provides them for the linear PBLG-POSS. The resonance of benzylic CH_2 group of N_3 -POSS connected to the azide unit (4.36 ppm) shifted downfield significantly to 5.56 ppm for POSS-*b*-PBLG. In addition, the signals for the isobutyl groups attached to silicon atoms of the POSS moiety appeared at about 0.63, 0.93, and 1.85 ppm and the proton on the nitrogen atom of PBLG resonated as a singlet at 7.9 ppm, confirming the synthesis of POSS-*b*-PBLG. Figure 5(b) reveals that the $C=O$ and amide carbon atom signals appear in the ^{13}C NMR spectrum of alkyne-PBLG at 172.3 and 171.4 ppm, respectively, while those of the phenyl ring appear at 136.4 ppm, with the other phenyl ring carbon atoms appearing as a signal at about 128 ppm. The signals for the benzylic carbon atom and the amino acid α -carbon atoms (NHCOC) appear at 66.0 and 52.0 ppm (β -sheet conformation), respectively. A small peak at 55.1 ppm arises from α -carbon atoms in the α -helix conformation. The signals of the alkyne carbon atoms of alkyne-PBLG appear at 81.0 and 73.4 ppm; Figure 5(a) provides assignments of the remaining signals for the carbon atoms of alkyne-PBLG. Figure 5(b)

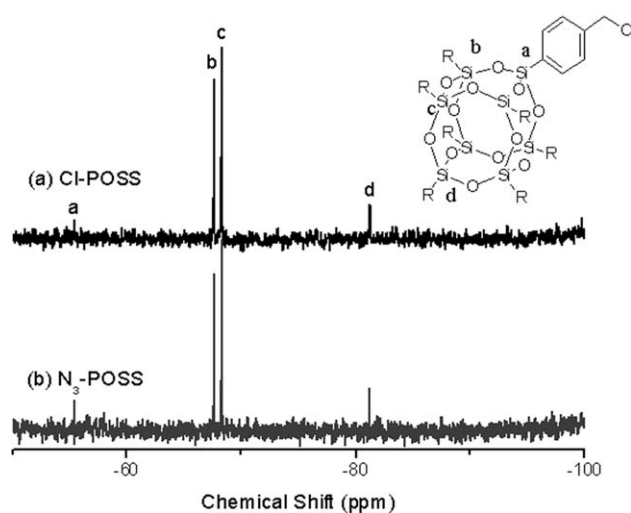


FIGURE 2 ^{29}Si NMR spectra of (a) Cl-POSS and (b) N_3 -POSS.

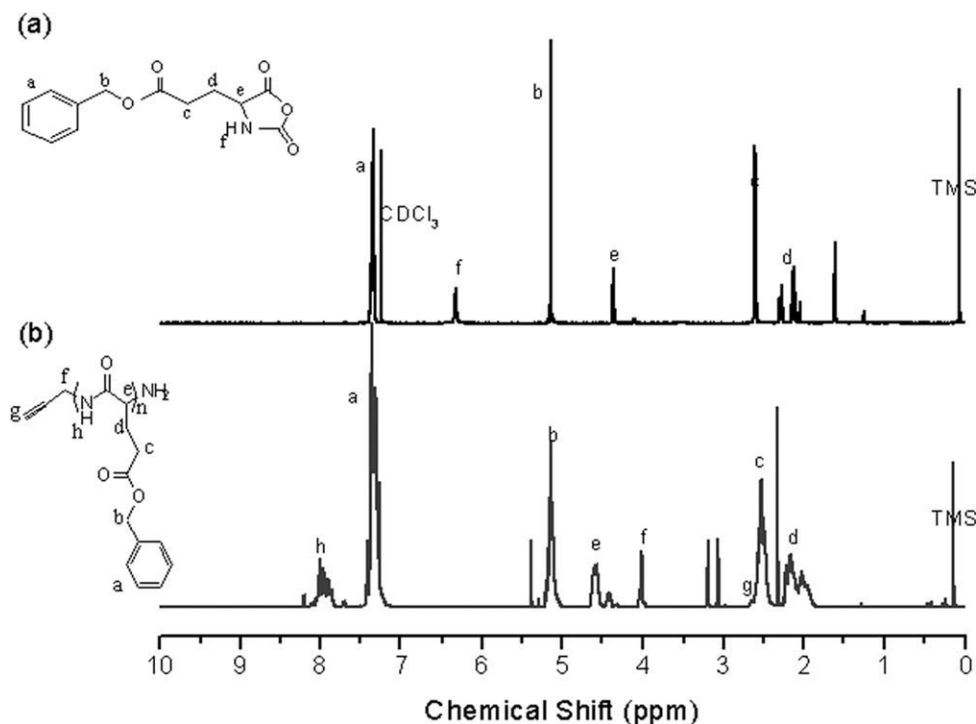


FIGURE 3 ¹H NMR spectra of (a) BLG monomer (in CDCl₃) and (b) alkyne-PBLG (in CDCl₃ and 15 wt % TFA).

displays the ¹³C NMR spectrum of POSS-*b*-PBLG. The signals for the alkyne carbon atoms are absent, but those of the isobutyl carbon atoms of the POSS moiety were present at 0.2, 25.0, and 29.0 ppm; Figure 5(b) provides assignments of all of the other signals for the carbon atoms of POSS-*b*-PBLG. FTIR spectroscopic analysis (Fig. 6) confirmed the complete disappearance of the characteristic signals for the azido and acetylene groups. The signal at 2105 cm⁻¹, corresponding to the absorbance of the azido group of N₃-POSS, was absent in the spectra of the linear POSS-*b*-PBLG; the absorption band of the Si—O—Si (siloxane) groups of the POSS moiety appears at 1100 cm⁻¹ in the spectra of the POSS-*b*-PBLG copolymers, indicating that the azido and acetylene function-

alities had participated in the click reactions. Taken together, the ¹H NMR, ¹³C NMR, and FTIR spectra all confirmed the successful synthesis of POSS-*b*-PBLG. Table 1 also lists the molecular weight of the various POSS-*b*-PBLG species, as determined through ¹H NMR spectroscopic and GPC analyses.

Thermal Analyses of POSS-*b*-PBLG Copolymers

Figure 7 presents DSC thermograms of the alkyne-PBLG and linear PBLG-*b*-POSS systems. During the second heating run of each of these systems, we observed only one glass

TABLE 1 Molecular Characteristics of the Alkyne-PBLG and POSS-*b*-PBLG Systems

Compound	M_n^a	M_n^b	M_w^b	PDI ^b	DP ^a
PBLG ₅	1,020	ND ^c	ND	ND	5
PBLG ₁₀	2,340	3,220	3,720	1.11	10
PBLG ₂₀	4,470	4,080	4,300	1.05	20
PBLG ₃₃	7,370	5,290	6,700	1.26	33
PBLG ₅₃	11,580	7,340	9,500	1.29	53
POSS- <i>b</i> -PBLG ₅	1,960	ND	ND	ND	5
POSS- <i>b</i> -PBLG ₁₀	3,300	4,050	4,520	1.12	10
POSS- <i>b</i> -PBLG ₂₀	5,400	5,000	5,500	1.10	20
POSS- <i>b</i> -PBLG ₃₃	8,300	5,800	7,300	1.26	33
POSS- <i>b</i> -PBLG ₅₃	12,500	8,760	10,800	1.24	53

^a Determined from ¹H NMR spectra.

^b Determined from GPC analysis.

^c Not detectable.

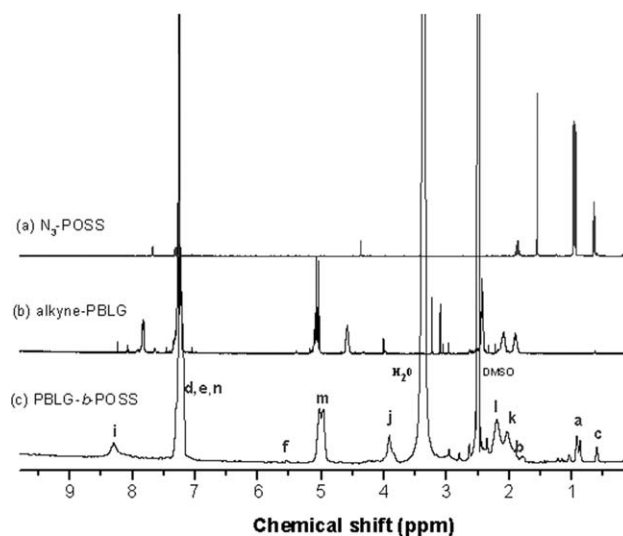


FIGURE 4 ¹H NMR spectra of (a) N₃-POSS (in CDCl₃), (b) alkyne-PBLG₅ (in CDCl₃), and (c) POSS-*b*-PBLG₅ (in d₆-DMSO).

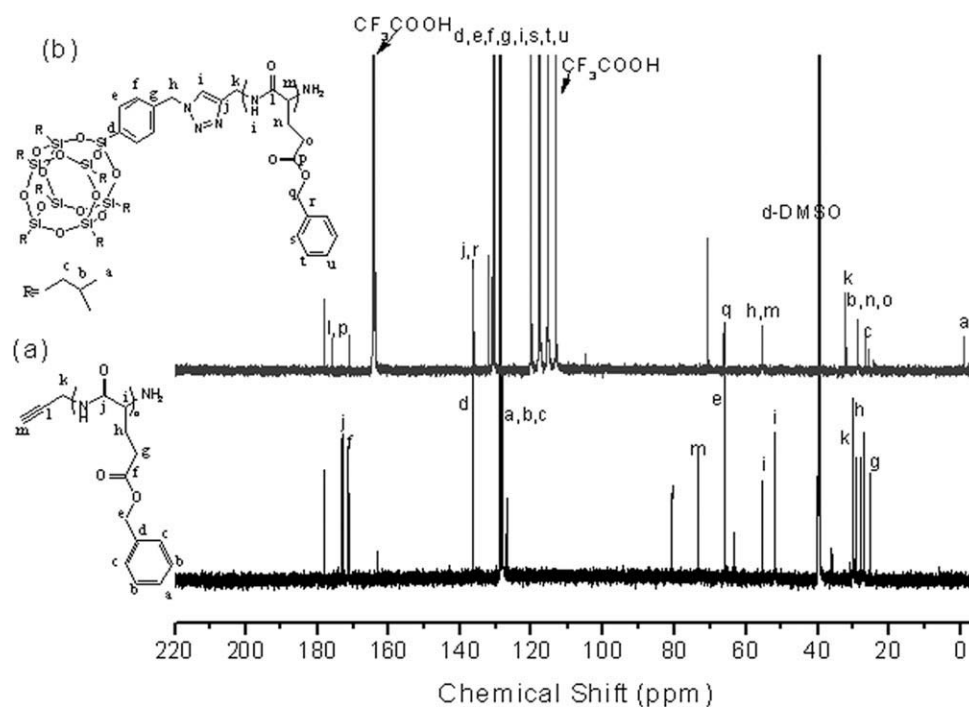


FIGURE 5 ^{13}C NMR spectra of (a) alkyne-PBLG₅ (in d_6 -DMSO) and (b) POSS-*b*-PBLG₅ (in TFA).

transition temperature (T_g , at ca. 20 °C), which increased upon increasing the degree of polymerization.³⁵ The glass transition behavior of the alkyne-PBLG and linear POSS-*b*-PBLG systems was almost identical; the value of T_g of the linear POSS-*b*-PBLG was higher (by ca. 4 °C) than that of the linear alkyne-PBLG only for the lowest molecular weight PBLG₅, presumably because the β -sheet conformation of alkyne-PBLG₅ transformed into a rigid rod-like α -helix structure after incorporation of the POSS unit into the linear POSS-*b*-PBLG₅ system (i.e., due to the larger POSS content in this block copolymer than in the other, higher molecular weight POSS-*b*-PBLG species). In the following section, we

characterize the transformations of the secondary structures of the alkyne-PBLG and linear POSS-*b*-PBLG systems, as determined through FTIR spectroscopy and WAXD analyses.

Conformational Study of the Peptide Segment

We recorded FTIR spectra at room temperature to obtain information regarding the conformations of the peptide segments in the alkyne-PBLG and linear POSS-*b*-PBLG systems (Fig. 8). Analysis using the second derivative technique¹¹ indicated that the amide I band at 1655 cm^{-1} was characteristic of the α -helical secondary structure. For polypeptides possessing a β -sheet conformation, the position of the amide I band is shifted to 1627 cm^{-1} , while that of a random coil or turn population is located at 1693 cm^{-1} ; the free C=O

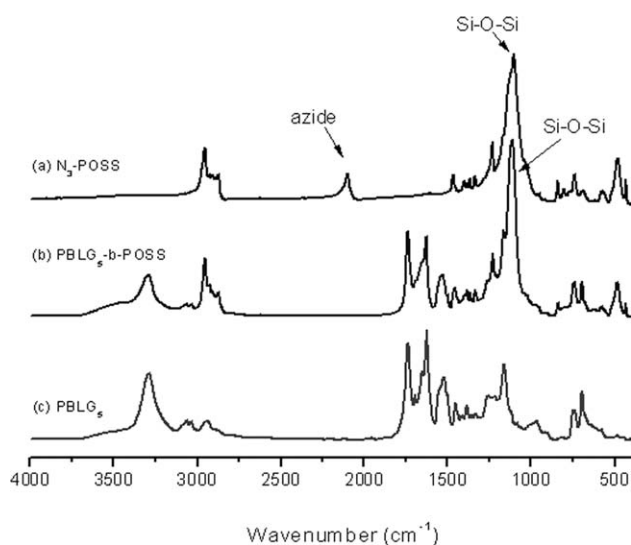


FIGURE 6 FTIR spectra of (a) N₃-POSS, (b) POSS-*b*-PBLG₅, and (c) alkyne-PBLG₅.

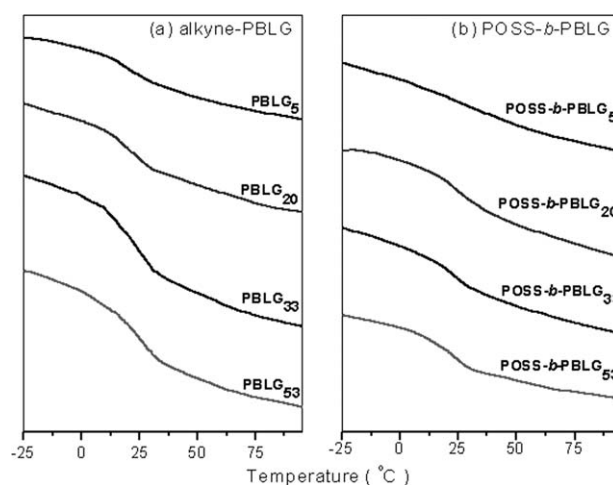


FIGURE 7 DSC traces (second heating runs) of (a) alkyne-PBLG and (b) POSS-*b*-PBLG.

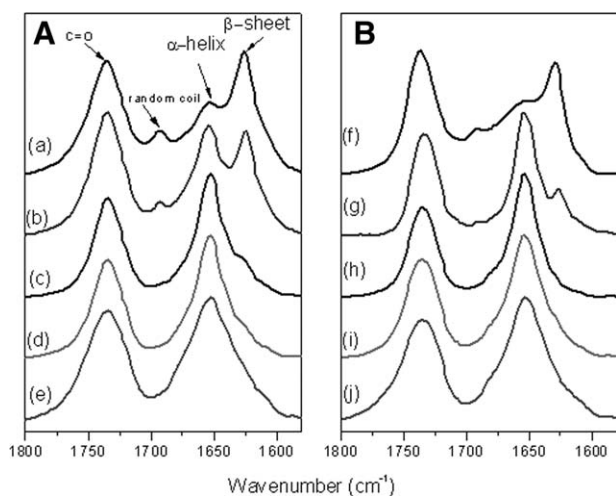


FIGURE 8 FTIR spectra of (A) alkyne-PBLG species incorporating for (a) PBLG₅, (b) PBLG₁₀, (c) PBLG₂₀, (d) PBLG₃₃, (e) PBLG₅₃ and (B) POSS-*b*-PBLG species incorporating (f) PLBG₅, (g) PLBG₁₀, (h) PLBG₂₀, (i) PLBG₃₃, and (j) PLBG₅₃.

unit of the side chain group of PBLG provided a signal at 1734 cm^{-1} , while the signals at 1607 and 1594 cm^{-1} represented stretching of the benzene units of the side chain groups of PBLG. Next, we used the deconvolution technique in a series of Gaussian distributions to quantify the fraction of each of the peaks (Fig. 9). Table 2 summarizes the results

of curve fitting of the signals for the amide I groups for the β -sheet, α -helical, and random coil structures; Figure 10 summarizes the results. The fraction of α -helical secondary structures increased on increasing the degree of polymerization in both the alkyne-PBLG and POSS-*b*-PBLG systems, similar to the findings reported by Papadopoulos et al.³⁵ At a low degree of polymerization ($DP < 20$), both secondary structures were present, but as the degree of polymerization increased, the α -helical secondary structure was favored. In addition, each of the linear POSS-*b*-PBLG systems obtained after performing the click reactions had a higher fraction of the α -helical secondary structure and lower fractions of β -sheet and random coil secondary structures than did its corresponding alkyne-PBLG system at the same degree of polymerization of the polypeptide.

We observed similar phenomena in the WAXD analyses at 393 K of the secondary structural changes of the alkyne-PBLG and POSS-*b*-PBLG systems (Fig. 11). Here, we discuss the effects of chain length and the incorporation of POSS on the secondary structure of PBLG. For the alkyne-PBLG species [Fig. 11(a)], the diffraction pattern of PBLG at a DP of 20 revealed the presence of two secondary structures. The first peak, at a value of 2θ of 4.57° , reflects the distance ($d = 1.67\text{ nm}$) between the backbones in the antiparallel β -pleated sheet structure; the second, at 16.2° ($d = 0.47\text{ nm}$) represents the intermolecular distance between adjacent peptide chains with one lamella. The three reflections at higher angles, with relative positions $1:3^{1/2}:4^{1/2}$, relative to

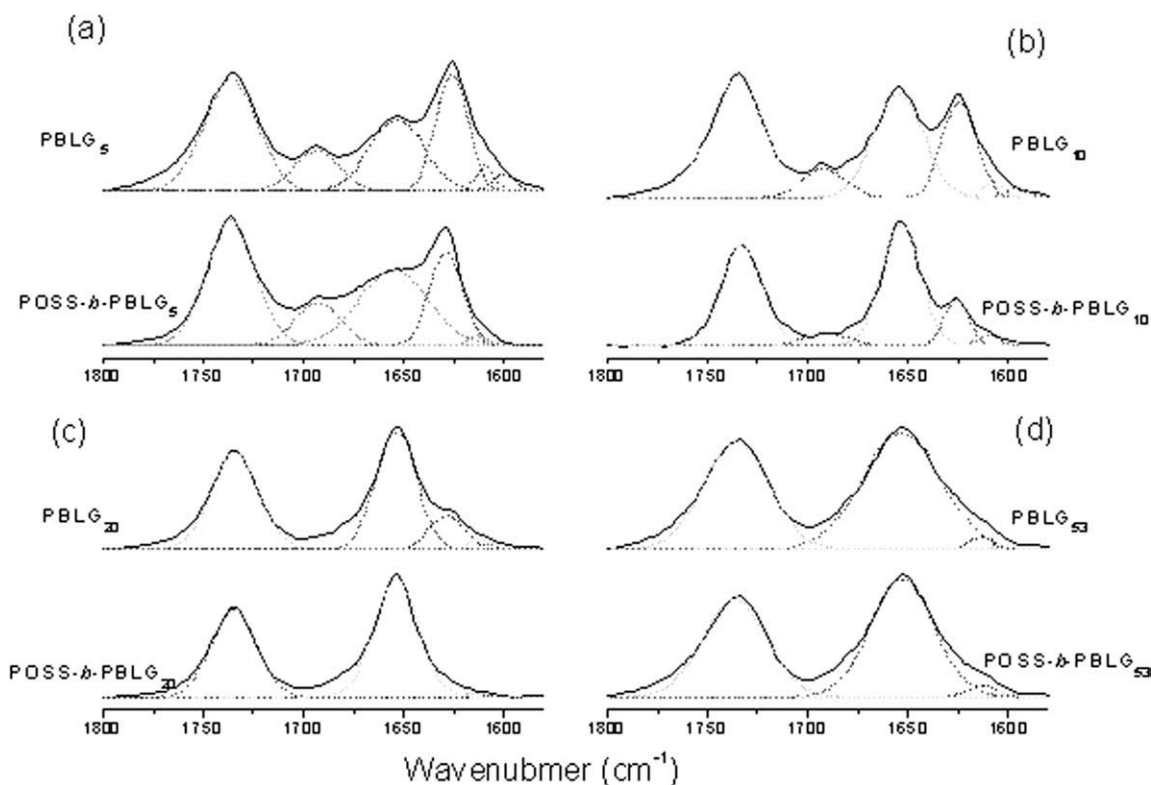


FIGURE 9 Curve fitting data from the analysis of the FTIR spectra of the alkyne-PBLG species incorporating (a) PBLG₅, (b) PBLG₁₀, (c) PBLG₂₀, and (d) PBLG₅₃, and their corresponding POSS-*b*-PBLG systems.

TABLE 2 Curve-Fitting of Secondary Structure of Alkyne-PBLG and Linear PBLG-*b*-POSS (ν : Wavenumber (cm^{-1}), $W_{1/2}$: Half-Width (cm^{-1}), A_f : Area Fraction of Each Peak)

Sample	Random Coil			α -Helix			β -Sheet		
	ν	$W_{1/2}$	A_f	ν	$W_{1/2}$	A_f	ν	$W_{1/2}$	A_f
PBLG ₅	1693	27	18.9	1653	32	41.3	1626	19	39.8
PBLG ₅ -POSS	1693	27	18.7	1654	32	51.5	1627	19	29.8
PBLG ₁₀	1692	26	12.6	1655	30	54.0	1625	20	33.4
PBLG ₁₀ -POSS	1691	27	8.8	1654	28	74.2	1626	18	17.0
PBLG ₂₀	1693	25	5.9	1654	26	76.1	1627	20	18.0
PBLG ₂₀ -POSS	–	–	0	1654	26	100	–	–	0
PBLG ₃₃	–	–	0	1653	28	100	–	–	0
PBLG ₃₃ -POSS	–	–	0	1652	30	100	–	–	0
PBLG ₅₃	–	–	0	1652	38	100	–	–	0
PBLG ₅₃ -POSS	–	–	0	1652	36	100	–	–	0

the primary peak at q^* , are indexed according to the (10), (11), and (20) reflections of a 2D hexagonal packing of cylinders composed of 18/5 α -helices with a cylinder distance of 1.36 nm.³⁵ The structure of PBLG has been as a nematic-like paracrystal with a periodic packing of α -helices in the direction lateral to the chain axis.⁴ The broad amorphous signal at about 16° originates mainly from the long amorphous side chain. Further increases in the DP of PBLG to 33 and 53 resulted in disappearance of the diffraction peak at 4.57° associated with the β -sheet secondary structure, suggesting the absence of that particular conformation for the longer peptides. In addition, the α -helical conformations were better packed for the longer peptides. Decreasing the length of the PBLG chain (DP = 5 and 10) led to destabilization of the α -helical secondary structures, causing the β -sheet secondary structures to be observed as signals at values of 2θ of 4.57° and 16° , respectively. These results are consistent with those from our FTIR spectroscopic analyses: For low DPs (<20), the alkyne-PBLG systems featured both secondary structures; as the DP increased, however, the α -helical secondary structure was favored.

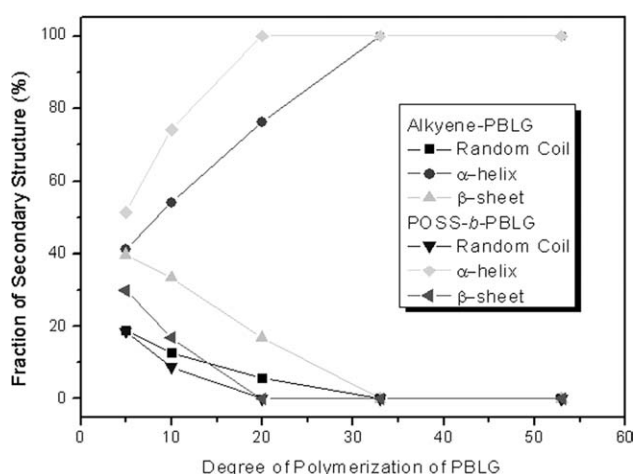
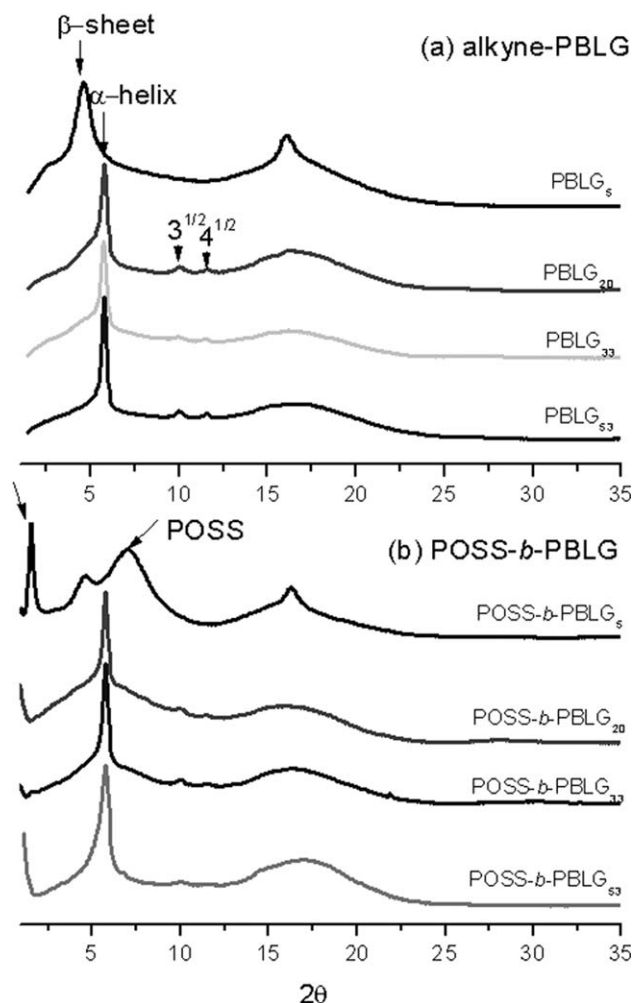
**FIGURE 10** Secondary structures of alkyne-PBLG and POSS-*b*-PBLG systems featuring different degrees of polymerization.

Figure 11(b) presents the WAXD patterns of the linear POSS-*b*-PBLG recorded at 393 K. For the linear POSS-*b*-PBLG species having longer PBLG segments (DP > 20), we observe

**FIGURE 11** WAXD patterns (recorded at 393 K) of (a) alkyne-PBLG and (b) POSS-*b*-PBLG species featuring with different degrees of polymerization.

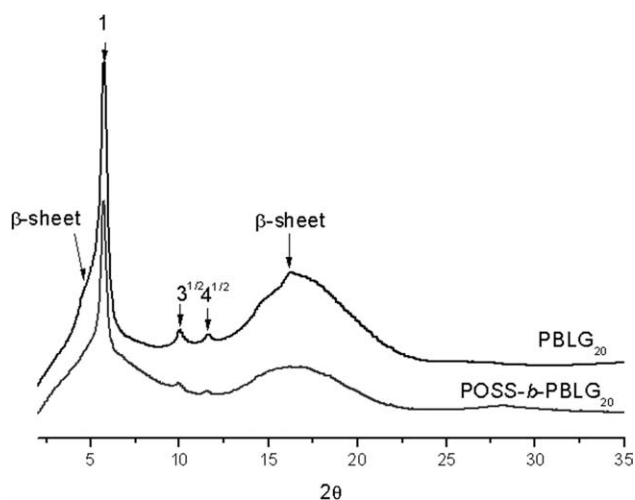


FIGURE 12 WAXD analyses of (a) alkyne-PBLG₂₀ and (b) POSS-*b*-PBLG₂₀ species.

only one set of Bragg peaks at diffraction angles having a ratio of $1:3^{1/2}:4^{1/2}$, indicating a columnar hexagonal arrangement of the molecules. On decreasing the length of the peptide segment ($DP < 20$) of the linear POSS-*b*-PBLG systems, a considerable fraction of the peptide segments featured a β -sheet secondary structure, similar to behavior of the corresponding alkyne-PBLG systems. Figure 12 summarizes the WAXD patterns of alkyne-PBLG₂₀ and POSS-*b*-PBLG₂₀. After performing the click reaction, POSS-*b*-PBLG₂₀ featured a higher fraction of α -helical secondary structures than did its precursor alkyne-PBLG₂₀. Therefore, it appears that even if peptides only partially adopt the α -helical and β -sheet conformations, when anchored to POSS in the form of a block polymer they undergo conformational stabilization such that most of the peptide segments are constrained in the α -helical secondary structure. In addition, Figure 11(b) reveals that the WAXD pattern of POSS-*b*-PBLG₅ features more two additional diffraction angles (at ca. 1.6° and 7.1°) relative to that of pure alkyne-PBLG₅, suggesting microphase separation into a lamellar-like sequence featuring a bilayer structure and (101) diffraction planes for hexagonal POSS crystals, respectively.

Gallot et al.^{36,37} used SAXS to investigate the morphologies of linear polyvinyl/polypeptide coil/rod block copolymers in the solid state. They found a large-scale hexagonal-in-lamellar morphology of alternating polyvinyl and polypeptide sheets with α -helical polypeptide chains arranged in a hexagonal array. To observe the correlation between the self-assembly of the hexagonally packed polypeptides and the crystallization of the POSS units, we conducted SAXS analyses of the POSS-*b*-PBLG systems (Fig. 13). The broad peak, assumed to be a Bragg reflection, at a value of q of 0.125 corresponds to an ordering spacing of about 50 Å for POSS-*b*-PBLG₅; this phenomenon is consistent with the WAXD data at a value of 2θ of 1.6° . Increasing the length of the PBLG chain resulted in a Bragg reflection at a value of q of 0.076, corresponding to an ordering spacing of about 82 Å for

POSS-*b*-PBLG₂₀. Structurally speaking, the PBLG tethers the POSS units from its crystalline domains; meanwhile, the scattered POSS moieties gather and lock into the copolymers to form crystalline entities. The cleaner system can now phase-separate into two different types of crystalline domains, which further pack into a lamellar-like sequence having a bilayer structure. The characteristic spacing (50 Å) observed from the SAXS data is consistent with the bilayer structure of the POSS-*b*-PBLG₅ copolymer [Scheme 3(a)]. The observed spacing is close to the thickness (50 Å) expected for the repeated packing of a “{POSS}-{PBLG₅ β -sheet}-{PBLG₅ β -sheet}-{POSS}” bilayer structure, as estimated from twice the sum of the POSS length ($2 \times 11 \text{ \AA}^2$) and peptide length ($2 \times 5 \times 3 \text{ \AA}^3$). For this calculation, we estimated the length of polypeptide segment by considering the β -sheet conformation to have a length of about 3 Å for each repeat unit, rather than the length of 3.8 Å expected for fully extended peptide bonds³⁸; we estimated the length of isobutyl-POSS to be about 11 Å from first diffraction peak at a value of 2θ of 7.1° . In addition, we would expect the observed spacing of the POSS-*b*-PBLG₂₀ copolymer to be 82 Å, for the repeated packing of a “{POSS}-{PBLG₂₀ α -helix}-{PBLG₂₀ α -helix}-{POSS}” bilayer structure, estimated from twice the sum of the POSS length ($2 \times 11 \text{ \AA}^2$) and the peptide length ($2 \times 20/3.6 \times 5.4 \text{ \AA}^3$), as indicated in Scheme 3(b). The length of the polypeptide segment was estimated by considering the 18/5 α -helical conformations to have a length of 5.4 Å for each pitch of the helix.

Figure 14 provides the thermal stabilities under N₂ of the POSS-*b*-PBLG₅ and alkyne-PBLG₅ nanocomposites. To compare their thermal stabilities, we used the 20 wt % weight loss temperature as a standard. We observe a significantly increased (ca. 80 °C) decomposition temperature (T_d) for POSS-*b*-PBLG₅ relative to that of alkyne-PBLG₅, presumably because of the nano-reinforcement effect of incorporating POSS moieties into polymeric matrices. A recent study demonstrated that POSS units can significantly retard thermal

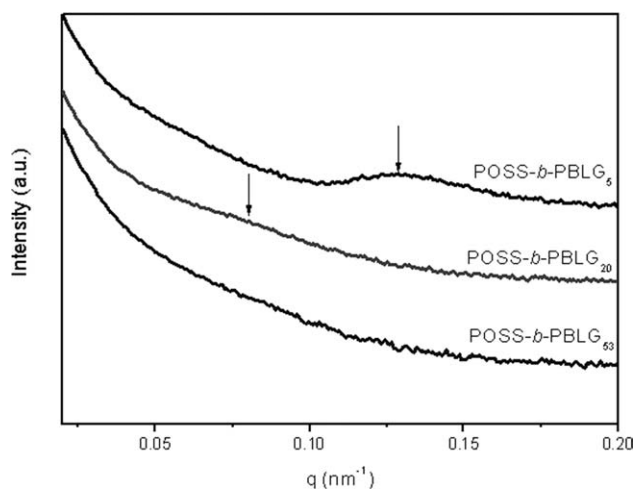
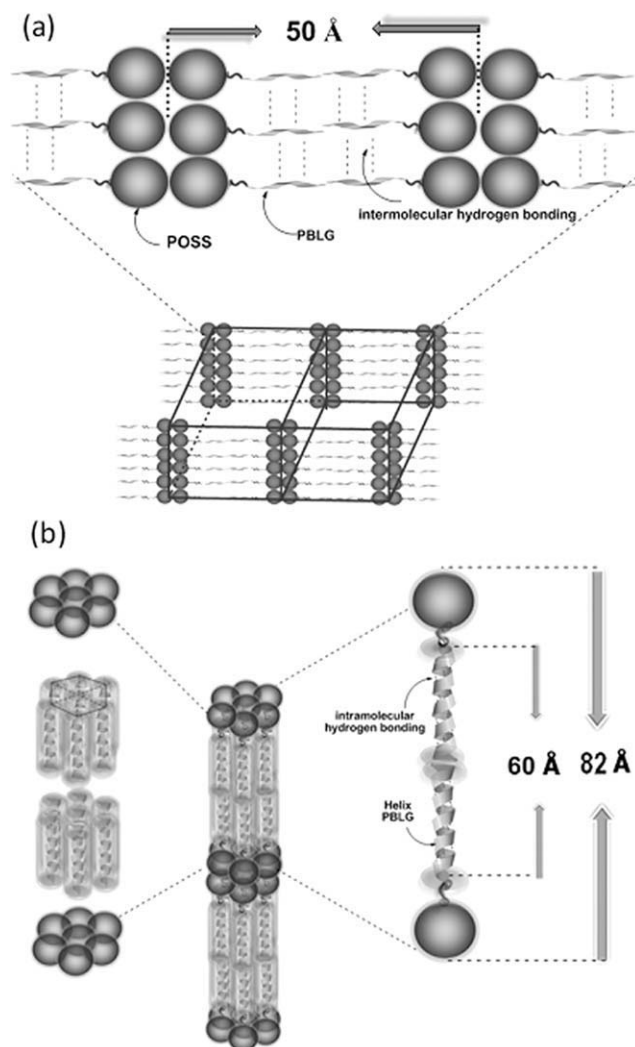


FIGURE 13 SAXS patterns (recorded at room temperature) of POSS-*b*-PBLG species incorporating different degrees of polymerization.



SCHEME 3 Proposed model for the self-assembly of the (a) POSS-*b*-PBLG₅ and (b) POSS-*b*-PBLG₂₀ copolymers.

motion; at the same time, they can act as flow aids at elevated temperatures. In addition, the increased values of T_d for the nanocomposites may also result from increased chain spacing, which gives rise to lower thermal conductivity.³⁹ In materials featuring POSS nanoparticles, thermal motion is restricted, thereby reducing the number of pathways for organic decomposition; the inorganic POSS component provides additional heat capacity, thereby stabilizing the materials against thermal decomposition. Char yield, another indicator of thermal stability, also increased after tethering the POSS nanoparticles. Thus, the thermal stability of PBLG improved as a result of the formation of network structures and because of the presence of the inorganic silsesquioxane.^{40–42}

EXPERIMENTAL

Materials

Isobutyltrisilanol-POSS was obtained from Hybrid Plastics. Propargylamine was purchased from Tokyo Kasei Kogyo. Copper(I) bromide (CuBr) was purified by washing with gla-

cial AcOH overnight, followed by washing with absolute EtOH and ethyl ether, and then drying under vacuum. *N,N*-Dimethylformamide (DMF), sodium azide (NaN₃), triethylamine (TEA), trichloro[4-(chloromethyl)phenyl]silane, and *N,N,N,N,N*-pentamethyldiethylenetriamine (PMDETA, 99%) were purchased from Aldrich. All solvents were distilled before use. γ -Benzyl-L-glutamate *N*-carboxyanhydride was prepared according to a literature procedure⁴³ and stored at -30 °C before use.

Mono-Benzyl Chloride POSS (Cl-POSS)

A solution of trichloro[4-(chloromethyl)phenyl]silane (1.00 mL, 5.61 mmol), isobutyltrisilanol-POSS (4.05 g, 5.11 mmol), and TEA (2.20 mL, 15 mmol) in dry tetrahydrofuran (THF, 30.0 mL) was stirred at room temperature for 7.5 h under Ar and then filtered to remove the precipitated NET₃·HCl. The clear THF solution was added dropwise into a beaker of MeCN and rapidly stirred. The resulting product was filtered off and dried under vacuum. (4.61 g, 80%).

¹H NMR (CDCl₃): δ 7.65 (d, 2H), 7.39 (d, 2H), 4.60 (s, 2H), 1.92–1.82 (m, 7H), 0.98–0.94 (m, 42H), 0.65–0.62 (m, 14H) ppm. ²⁹Si NMR (CDCl₃): δ -55.44, -67.61, -68.27, -81.27 ppm. FTIR (KBr, cm⁻¹): 2956 m, 2871 m, 1465 m, 1400 w, 1366 w, 1332 w, 1230 m, 1110 vs, 1039 m, 838 m, 741 m, 694 w.

Mono-Benzyl Azide POSS (MBA-POSS, N₃-POSS)

NaN₃ (1.10 g, 16.9 mmol) was added to a solution of mono-benzyl chloride POSS (1.62 g, 1.72 mmol) in DMF (40 mL) and then the mixture was heated at 80 °C overnight. After cooling to room temperature, the mixture was diluted with CHCl₃ (150 mL) and washed with 1 M NaHCO₃ (2 × 100 mL) and water (2 × 100 mL). The organic layer was dried (Na₂SO₄) and the solvent evaporated under vacuum to yield a white solid (1.14 g, 70%).

¹H NMR (CDCl₃): δ 7.67 (d, 2H), 7.32 (d, 2H), 4.36 (s, 2H), 1.92–1.82 (m, 7H), 0.98–0.94 (m, 42H), 0.65–0.62 (m, 14H) ppm. ²⁹Si NMR (CDCl₃): δ -55.44, -67.61, -68.26, -81.19.

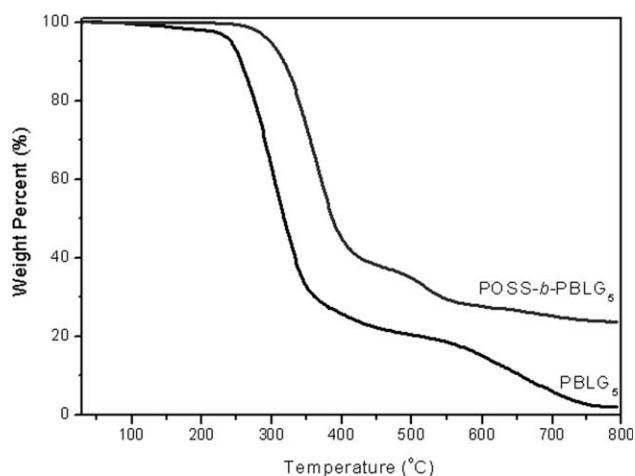


FIGURE 14 TGA analyses of alkyne-PBLG₅ and POSS-*b*-PBLG₅ species.

FTIR (KBr, cm^{-1}): 2956 s, 2871 m, 2102 m, 1465 m, 1399 w, 1383 w, 1366 w, 1334 w, 1230s, 1106 vs, 1038 m, 838 m, 803 w, 744 m. MALDI-TOF mass: 951 (g/mol).

Propargyl-Terminated PBLG³³

Bz-L-GluNCA (4.00 g, 15.2 mmol) was weighed in a dry-box under pure Ar, placed in a flame-dried Schlenk tube, and dissolved in anhydrous DMF (40 mL). The solution was stirred for 10 min and then propargylamine (12 μL , 175.2 μmol) was added using a N_2 -purged syringe. After stirring for 40 h at room temperature, the polymer was recovered through precipitation in diethyl ether and drying under high vacuum.

^1H NMR (CDCl_3): δ 7.84 (s, 1H, NH), 7.35 (m, 5H, ArH), 5.1 (d, 2H, CH_2Ar), 4.59 (s, 1H), 3.99 (d, 2H), 2.45 (d, 2H), 2.18 (s, 1H), 2.10–1.90 (m, 2H).

PBLG-*b*-POSS Diblock Copolymers

N_3 -POSS (0.15 g, 0.158 mmol), alkyne-PBLG (0.09 g, 0.028 mmol), and CuBr (3.59 mg, 0.025 mmol) were dissolved in DMF (15 mL) in a flask equipped with a magnetic stirrer bar. After one brief freeze/thaw/pump cycle, PMDETA (5.27 μL , 0.025 mmol) was added; the reaction mixture was then carefully degassed through three freeze/thaw/pump cycles, placed in an oil bath thermostated at 60 $^\circ\text{C}$, and stirred for 24 h. After evaporating all of the solvent under reduced pressure, the residue was dissolved in CH_2Cl_2 and passed through a neutral alumina column to remove copper catalysts. Evaporating of the solvent yielded the linear PBLG-*b*-POSS as a dark powder.

Characterization

^1H NMR spectra were recorded at room temperature using a Bruker AM 500 (500 MHz) spectrometer; with the residual proton resonance of the deuterated solvent acting as the internal standard. Molecular weights and molecular weight distributions were determined through gel permeation chromatography (GPC) using a Waters 510 high-performance liquid chromatograph (HPLC) equipped with a 410 differential refractometer and three Ultrastayragel columns (100, 500, and 10^3 \AA) connected in series, with dimethylacetamide (DMAc) as the eluent (flow rate: 0.4 mL/min). Thermal analysis through differential scanning calorimetry (DSC) was performed using a TA-Q20 operated at a scan rate of 10 $^\circ\text{C}/\text{min}$ over a temperature range from -90 to 120 $^\circ\text{C}$ under a N_2 atmosphere. The thermal stability of the samples was characterized using a TA Q-50 thermogravimetric analyzer operated under a N_2 atmosphere. The cured sample (ca. 7 mg) was placed in a Pt cell and heated at a rate of 20 $^\circ\text{C}/\text{min}$ from 30 to 800 $^\circ\text{C}$ under a N_2 flow rate of 60 mL/min. FTIR spectra of the polymer films were recorded using the conventional KBr disk method. The films used in this study were sufficiently thin to obey the Beer-Lambert law. FTIR spectra were recorded using a Bruker Tensor 27 FTIR spectrophotometer; 32 scans were collected at a spectral resolution of 1 cm^{-1} . Because polymers containing amide groups are hygroscopic, pure N_2 gas was used to purge the spectrometer's optical box to maintain dry sample films. X-ray diffraction (XRD) data were collected on the wiggler beamline BL17A1 of the National Synchrotron Radiation Research Center

(NSRRC), Taiwan. A triangular bent Si (111) single crystal was employed to obtain a monochromated beam having a wavelength (λ) of 1.3344 \AA . The XRD patterns were collected using a imaging plate (IP; Fuji BAS III; area = $20 \times 40 \text{ cm}^2$) curved with a radius equivalent to the sample-to-detector distance (280 mm). The two-dimensional (2D) XRD patterns observed for the sample (typical diameter: 10 mm; thickness: 1 mm) were circularly averaged to obtain a one-dimensional (1D) diffraction profile $I(Q)$, with the value of Q calibrated using standard samples of Ag-Behenate and Si powder (NBS 640b). SAXS experiments were performed using the SWAXS instrument at the BL17B3 beamline of the NSRRC, Taiwan; the X-ray beam had a diameter of 0.5 mm and a wavelength (λ) of 1.24 \AA . The blend samples (thickness: 1 mm) were sealed between two thin Kapton windows (thickness: 80 μm) and analyzed at room temperature.

CONCLUSIONS

We have prepared well-defined linear POSS-*b*-PBLG copolymers through ROP of Glu-NCA followed by click reactions with a monofunctional azide-POSS. After attaching the PBLG blocks to the POSS nanoparticles, the fraction of α -helical secondary structures increased as a result of intramolecular hydrogen bonding between the POSS and PBLG moieties. The POSS-*b*-PBLG systems exhibited greater conformation stability and superior thermal properties relative to those of pure PBLG. The self-assembly of POSS-*b*-PBLG formed a bilayer-like nanostructure featuring α -helical or β -sheets and POSS aggregates, as evidenced using SAXS analysis.

This study was supported financially by the National Science Council, Taiwan, Republic of China, under contracts NSC 97-2221-E-110-013-MY3 and NSC 97-2120-M-009-003. The WAXD experiments were conducted at the 17A1 beamline at the NSRRC, Taiwan.

REFERENCES AND NOTES

- Bae, Y.; Fukushima, S.; Harada, A.; Kataoka, K. *Angew Chem Int Ed* 2003, 42, 4640–4643.
- Klok, H. A.; Lecommandoux, S. *Adv Mater* 2001, 13, 1217–1229.
- Tang, H.; Zhang D. *J Polym Sci Part A: Polym Chem* 2010, 48, 2340–2350.
- Habraken, G. J. M.; Koning, C. E.; Heise, A. *J Polym Sci Part A: Polym Chem* 2009, 47, 6883–6893.
- Flory, P. J. *Proc R Soc London Ser A* 1956, 234, 73–89.
- Robinson, C.; Ward, J. C. *Nature* 1957, 180, 1183–1184.
- Yu, S. M.; Conticello, V. P.; Zhang, G.; Kayser, C.; Fournier, M. J.; Mason, T. L.; Tirrell, D. A. *Nature* 1997, 389, 167–170.
- Tohyama, K.; Miller, W. G. *Nature* 1981, 289, 813–814.
- Kuo, S. W.; Lee, H. F.; Chang, F. C. *J Polym Sci Part A: Polym Chem* 2008, 46, 3108–3119.
- Gitsas, A.; Floudas, G.; Mondeshki, M.; Spiess, H. W.; Aliferis, T.; Iatrou, H.; Hadjichristidis, N. *Macromolecules* 2008, 41, 8072–8080.

- 11** Sanchez-Ferrer, A.; Mezzenga, R. *Macromolecules* 2010, 43, 1093–1100.
- 12** Zhou, Q. H.; Zheng, J. K.; Shen, Z. H.; Fan, X. H.; Chen, X. F.; Zhou, Q. F. *Macromolecules* 2010, 43, 5367–5646.
- 13** Lee, H. F.; Sheu, H. S.; Jeng, U. S.; Huang, C. F.; Chang, F. C. *Macromolecules* 2005, 38, 6551–6558.
- 14** Papadopoulos, P.; Floudas, G.; Schnell, I.; Aliferis, T.; Iatrou, H.; Hadjichristidis, N. *Biomacromolecules* 2005, 6, 2352–2361.
- 15** Rao, J.; Zhang, Y.; Zhang, J.; Liu, S. *Biomacromolecules* 2008, 9, 2586–2593.
- 16** Ibarboure, E.; Papon, E.; Rodriguez-Hernandez, J. *Polymer* 2007, 48, 3717–3725.
- 17** Ibarboure, E.; Rodriguez-Hernandez, J. *J Polym Sci Part A: Polym Chem* 2006, 44, 4668–4679.
- 18** Klok, H. A.; Langenwalter, J. F.; Lecommandoux, S. *Macromolecules* 2000, 33, 7819–7826.
- 19** Lecommandoux, S.; Achard, M. F.; Langenwalter, J. F.; Klok, H. A. *Macromolecules* 2001, 34, 9100–9111.
- 20** Crespo, J. S.; Lecommandoux, S.; Borsali, R.; Klok, H. A.; Soldi, V. *Macromolecules* 2003, 36, 1253–1256.
- 21** Papadopoulos, P.; Floudas, G.; Schnell, I.; Lieberwirth, I.; Nguyen, T. Q.; Klok, H. A. *Biomacromolecules* 2006, 7, 618–626.
- 22** You, Y.; Chen, Y.; Hua, C.; Dong, C. M. *J Polym Sci Part A: Polym Chem* 2010, 48, 709–718.
- 23** Kuo, S. W.; Lee, H. F.; Huang, W. J.; Jeong, K. U.; Chang, F. C. *Macromolecules* 2009, 42, 1619–1626.
- 24** Xu, H.; Kuo, S. W.; Lee, J. S.; Chang, F. C. *Macromolecules* 2002, 35, 8788–8793.
- 25** Li, G. Z.; Wang, L. C.; Ni, H. L.; Pittman, C. U. *J Inorg Organometal Polym* 2001, 11, 123–154.
- 26** Mark, J. E. *Acc Chem Res* 2004, 37, 946–953.
- 27** Pielichowski, K.; Niuguna, J.; Janowski, B.; Pielichowski, J. *Adv Polym Sci* 2006, 201, 225–296.
- 28** Kuo, S. W.; Wu, Y. C.; Lu, C. H.; Chang, F. C. *J Polym Sci Part B: Polym Phys* 2009, 47, 811–819.
- 29** Huang, K. W.; Tsai, L. W.; Kuo, S. W. *Polymer* 2009, 50, 4876–4887.
- 30** Lu, C. H.; Kuo, S. W.; Chang, F. C. *Macromol Rapid Commun* 2009, 30, 2121–2127.
- 31** Lu, C. H.; Kuo, S. W.; Huang, C. F.; Chang, F. C. *J Phys Chem C* 2009, 113, 3517–3524.
- 32** Yen, Y. J.; Kuo, S. W.; Huang, C. F.; Chen, J. K.; Chang, F. C. *J Phys Chem B* 2008, 112, 10821–10829.
- 33** Kuo, S. W.; Tsai, H. T. *Polymer* 2010, 51, 5695–5704.
- 34** Zeng, K.; Zheng, S. *Macromol Chem Phys* 2009, 210, 783–791.
- 35** Papadopoulos, P.; Floudas, G.; Klok, H. A.; Schnell, I.; Pakula, T. *Biomacromolecules* 2004, 5, 81–91.
- 36** Billot, J. P.; Douy, A.; Gallot, B. *Makromol Chem* 1977, 178, 1641–1650.
- 37** Douy, A.; Gallot, B. *Polymer* 1982, 23, 1039–1044.
- 38** Voet, D.; Voet, J. G. *Biochemistry*; Hoboken, NJ: Wiley, 2004; p 227.
- 39** Turri, S.; Levi, M. *Macromolecules* 2005, 38, 5569–5574.
- 40** Lin, H. C.; Kuo, S. W.; Huang, C. F.; Chang, F. C. *Macromol Rapid Commun* 2006, 27, 537–541.
- 41** Wu, Y. C.; Kuo, S. W. *Polymer* 2010, 51, 3948–3955.
- 42** Huang, K. W.; Kuo, S. W. *Macromol Chem Phys* 2010, 211, 2301–2311.
- 43** Daly, W. H.; Poche, D. *Tetrahedron Lett* 1988, 29, 5859–5862.